Magnetic Resonance Imaging 56 (2019) 174–180

Contents lists available at ScienceDirect

Magnetic Resonance Imaging

journal homepage: www.elsevier.com/locate/mri

Original contribution

T_1–D–T_2 correlation of porous media with compressed sensing at low-field NMR

Yan Zhang[a], Lizhi Xiao[a,b,*], Xin Li[c], Guangzhi Liao[a]

[a] State Key Laboratory of Petroleum Resources and Prospecting, China University of Petroleum, Beijing 102249, China
[b] Harvard SEAS-CUPB Joint Laboratory on Petroleum Science, Cambridge, MA 02138, USA
[c] Sinopec Research Institute of Petroleum Engineering, Beijing, China

ABSTRACT

3D Laplace NMR can distinguish different components of confined fluid in sedimentary rocks, which is important to oil industry. However, the measurement time for such experiments is very long, which hinders the application in some cases such as NMR well logging. In this research, we accelerated T_1–D–T_2 experiment with compressed sensing (CS) method at low-field NMR. Simulation was first performed to examine the CS reconstruction method. The experiments were subsequently implemented on a 2 MHz spectrometer (Oxford instrument), which has a similar magnetic field strength to well logging tool. The T_1, D and T_2 information are obtained by the inversion recovery, pulsed field gradients and Carr–Purcell–Meiboom–Gill (CPMG) method, respectively. The subsampling is applied in T_1 and D dimensions with pseudo-random sampling. The measurement time reduced from 3 h to 0.6 h with CS method and a relative error of around 5% is achieved for data with signal-to-noise ratio of 28. The water and oil peaks are clearly distinguished in the correlation maps from subsampled data. The samples with different oil-water ratio and glass bead volume fraction were measured to examine the sensitivity of this method. In addition, diffusion and relaxation properties of the correlation maps are discussed.

1. Introduction

Nuclear Magnetic Resonance (NMR) technique has been applied to petroleum industry more than 60 years [1–3]. Abundant information can be acquired about the reservoir by NMR down-hole tool, such as porosity, permeability and fluid saturation [4,5]. For instance, relaxation (T_2, T_1) measurement of sedimentary rock provides the pore body diameter distribution [6,7]. Free water, capillary bound water and clay bound water in rocks can be distinguished using T_2 cutoff times [8]. Permeability can also inversed from T_2 distribution with proper model such as the Timur-Coates and SDR models [9,10]. In laboratory, rock core analysis was performed with NMR spectrometer [11,12]. Mitchell et al. monitored oil recovery process in real time with low-field NMR and discussed its application in core analysis [13]. Li et al. measured 3D oil distribution with π-EPI MRI technique at 0.2 T field strength for glass-bead pack and Spynie core plug samples [14]. NMR and MRI methods were also used to investigate low salinity waterflooding influence on enhanced oil recovery [15]. Since the fast 2D inverse Laplace transformation algorithm was proposed by Venkataramanan in 2002, 2D and 3D Laplace NMR methods is booming in oil industry [16]. Hürlimann et al. implemented diffusion (D)–T_2 correlation experiment to identify different fluids in sandstone [17]. Song et al. utilized T_1–T_2 correlation spectra to characterize pore environment in sandstone [18]. Sun et al. obtained D–T_1–T_2 correlation map using a global inversion method to distinguish oil and water in sandstone [19]. T_2–D– internal gradients correlation was also acquired with pulsed field gradient (PFG) to examine wettability [20]. However, 3D Laplace NMR is time-consuming, which limits the application in petroleum industry, especially in NMR well logging.

Nonuniform sampling has been widely used to accelerate NMR experiments [21,22]. In this research, we speeded T_1–D–T_2 correlation with compressed sensing (CS) at 2 MHz core analyzer. Details about the CS method were described in another paper [23].

2. Method

The T_1–D–T_2 signal attenuation can be expressed as the following equation:

$$M(t_d, G, t_{acq})/M_0 = \iiint d(1/T_1)dDd(1/T_2)f(1/T_1, D, 1/T_2)[1 - 2\exp(-t_d/T_1)] \exp[-D\gamma^2G^2\delta^2(\Delta - 1/3\delta)] \exp(-t_{acq}/T_2), \quad (1)$$

where $f(1/T_1,D,1/T_2)$ is the diffusion relaxation correlation function, $t_{acq} = nt_{E2}$, δ is the duration of the pulsed field gradient, Δ is the diffusion time, γ is the gyro-magnetic ratio, G is the amplitude of the gradient pulse, and t_d is the recovery time. The CS method is used to accelerate this experiment, which is achieved by solving the l_1

* Corresponding author at: China University of Petroleum – Beijing, Fuxue Rd. 18, Changping District, Beijing 102249, China.
E-mail address: xiaolizhi@cup.edu.cn (L. Xiao).

https://doi.org/10.1016/j.mri.2018.09.028
Received 29 July 2018; Received in revised form 25 September 2018; Accepted 26 September 2018

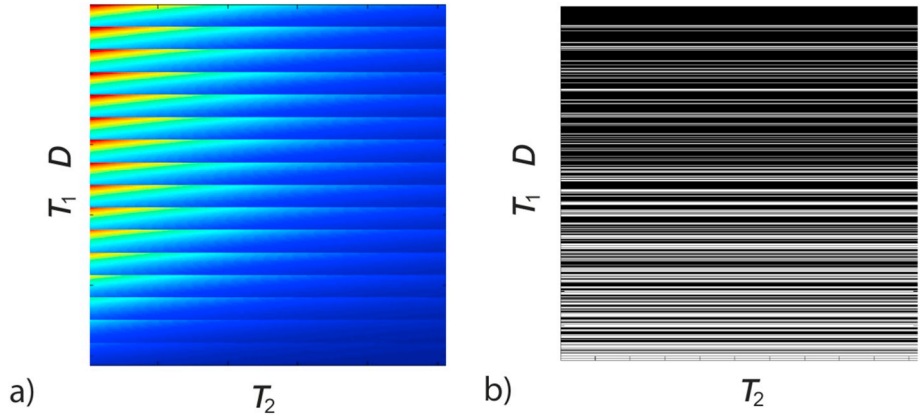

Fig. 1. (a) is the rearranged 3D data and (b) is the subsampling scheme, where the black lines represent sampled data.

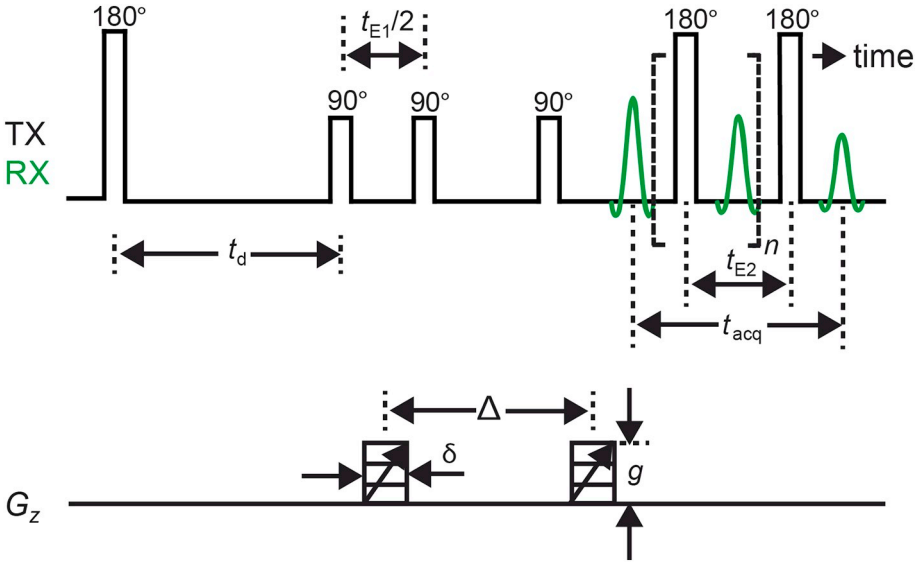

Fig. 2. Pulse sequence for T_1–D–T_2 experiment.

optimization problem:

$$\mathrm{argmin}_M(\|FM - b\|_2^2 + \lambda \|\Psi M\|_1) \quad (2)$$

where F is the subsampled operator, b is the subsampled data, Ψ is the sparse basis (the two-dimensional six-level Daubechies-3 wavelet basis in this research), λ is the regularization number, and M is the reconstructed fully sampled data. For the experiment mentioned above, subsampling can be only realized in the indirect domain (T_1 and D), which is shown in Fig. 1. The 3D data is rearranged to a 2D data before applying the CS reconstruction. The F is shown in Fig. 1b and the pseudo-random subsampling is employed in the T_1, D dimensions [22]. The accuracy of CS reconstruction is evaluated by the normalized relative error between original fully sampled data and reconstructed fully sampled data.

The 3D inverse Laplace transformation is then applied for the reconstructed data to obtain T_1–D–T_2 correlation maps. The rearranged 2D matrix form of Eq. 1 is:

$$M = K_{12} F K_3', \quad (3)$$

where $M \in \Re^{(N1\times N2)\times N3}$, $K_{12} \in \Re^{(N1\times N2)\times(Nx\times Ny)}$, $K_3 \in \Re^{N3\times Nz}$, $F \in \Re^{(Nx\times Ny)\times Nz}$, and $\varepsilon \in \Re^{(N1\times N2)\times N3}$. $K_{12} = K_1 \otimes K_2$. K_1, K_2, K_3, F, and M are the matrix form of $[1\text{-}2\exp(-t_d/T_1)]$, $\exp.[-D\gamma^2G^2\delta^2(\Delta\text{-}\delta/3)]$, $\exp.(-t_{acq}/T_2)$ and $f(1/T_1,D,1/T_2)$ respectively. To suppress the data, singular value decomposition is applied to the K_{12} and K_3 matrices: $K_{12} = U_{12}\,\Sigma_{12}\,V_{12}$ and $K_3 = U_3\,\Sigma_3\,V_3$. Then the Eq. (3) can be rewritten as:

$$\widetilde{M} = \widetilde{K}_{12} F \widetilde{K}_3' \quad (4)$$

where $\widetilde{M} = U_{12}' M U_3$, $\widetilde{K}_{12} = U_{12}' K_{12}$, $\widetilde{K}_3 = U_3' K_3$. With this reduced form of matrices, fast 3D Laplace inversion can be achieved by the nonnegative least square regularization method:

$$\mathrm{argmin}_{F>0}(\|\widetilde{M} - \widetilde{K}_{12} F \widetilde{K}_3^1\|^2 + \|\widetilde{M}\|^2) \quad (5)$$

3. Experiments and simulations

Glass-bead sample with diameter of 100 μm was measured, which was saturated with water and two kinds of oil (peanut and salad oil). To examine the sensitivity of this method, the oil-water mixture ratio is set to 1:1 and 1:2, and the volume proportion of glass beads is set to 0.56 (loose packing) and 0.64 (dense packing). The dense packing is achieved by the following procedure: the glass-bead container is vacuumed 2 h and then water is filled with 5 MPa pressure. The experiments were implemented on a 2 MHz spectrometer (Oxford instrument). The pulse sequence is shown in Fig. 2. The T_1 information is encoded with the inversion recovery method and t_d is increased logarithmically from 1 ms to 2 s in 30 steps. The diffusion information was acquired by stimulated echo with pulsed field gradients. The strength of applied gradients was varied linearly from 0 to 0.5 T/m in 30 steps. The T_2 relaxation was measured by Carr–Purcell–Meiboom–Gill (CPMG)

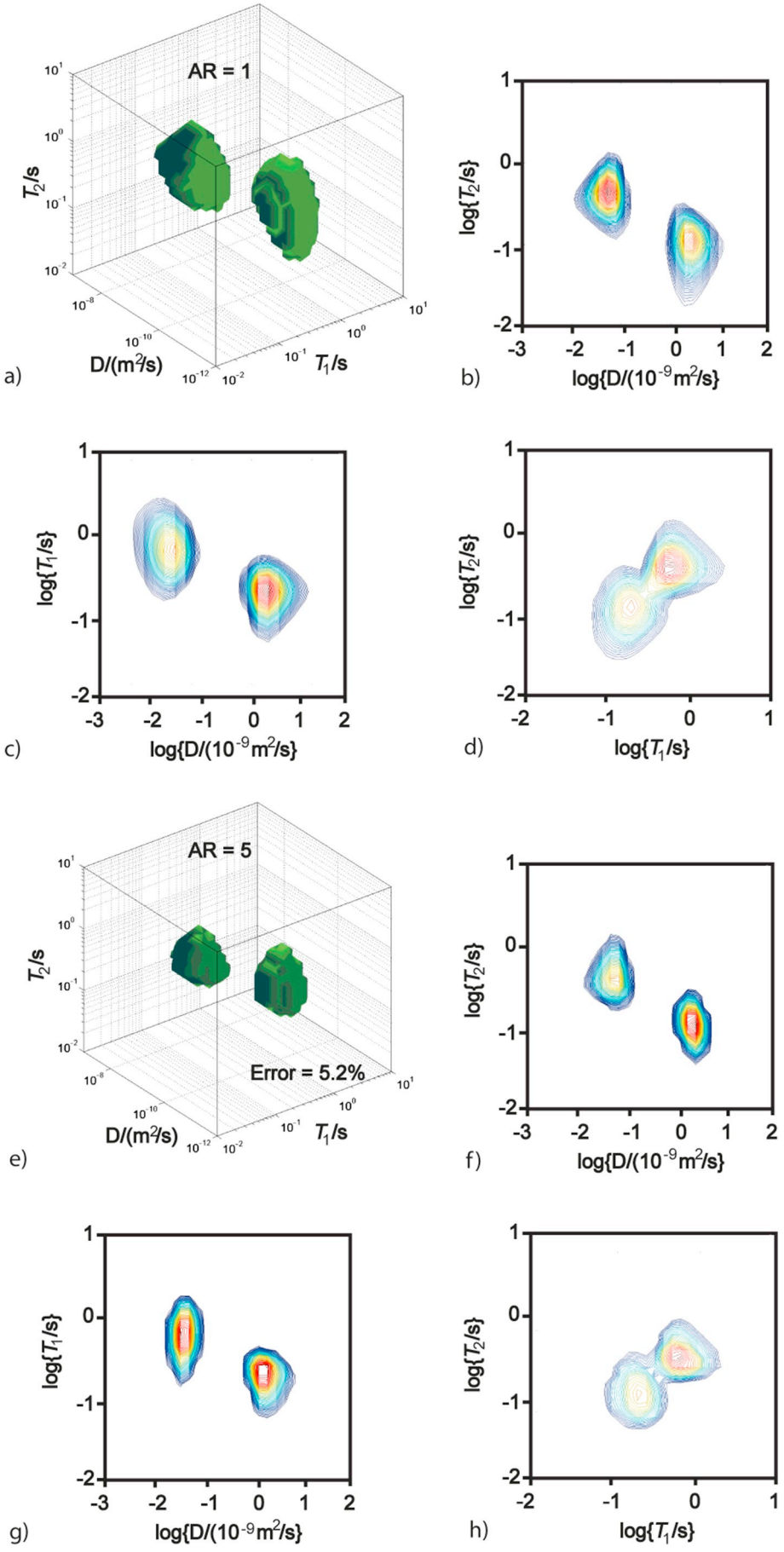

Fig. 3. Simulation results: (a)–(d) inversed from fully sampled data. (e)–(h) inversed from subsampled data.

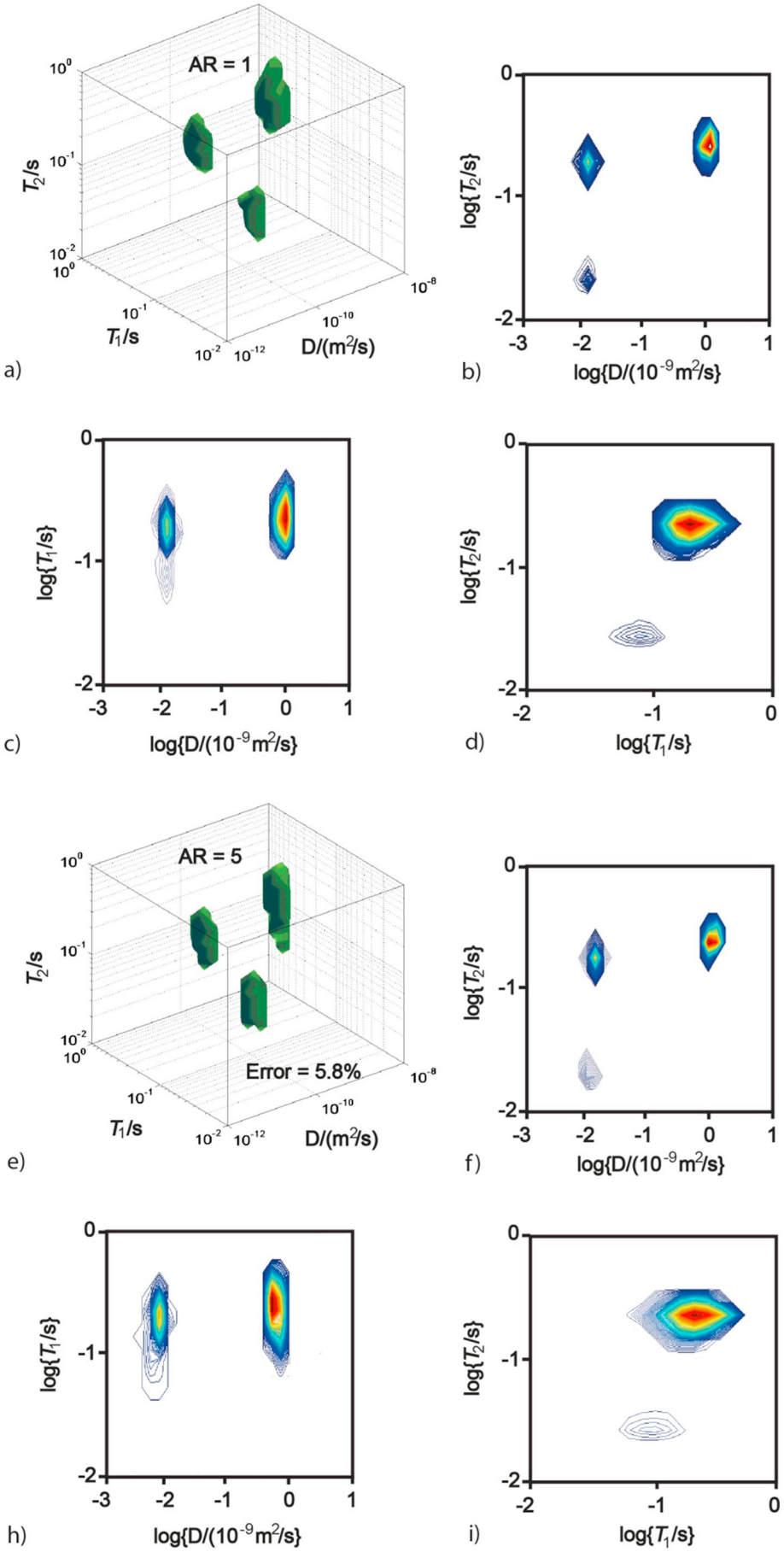

Fig. 4. Experimental results (a)–(d) spectra from fully sampled data. (e)–(h) spectra from subsampled data. The SNR is 28. The oil-water mixture ratio is 1:2 and the glass bead volume fraction is 0.56.

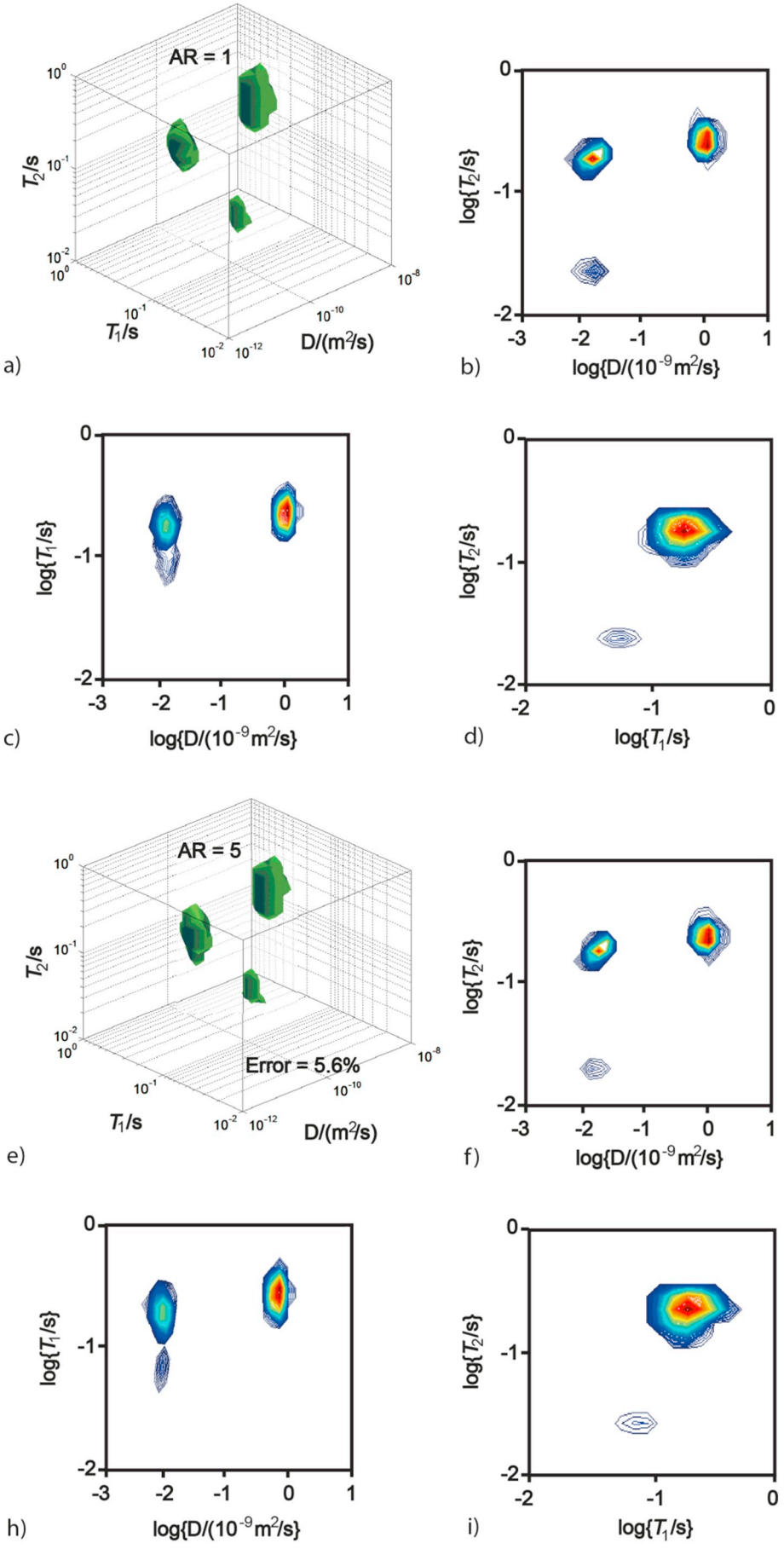

Fig. 5. Experimental results (a)–(d) spectra from fully sampled data. (e)–(h) spectra from subsampled data. The SNR is 29. The oil-water mixture ratio is 1:1 and the glass bead volume fraction is 0.56.

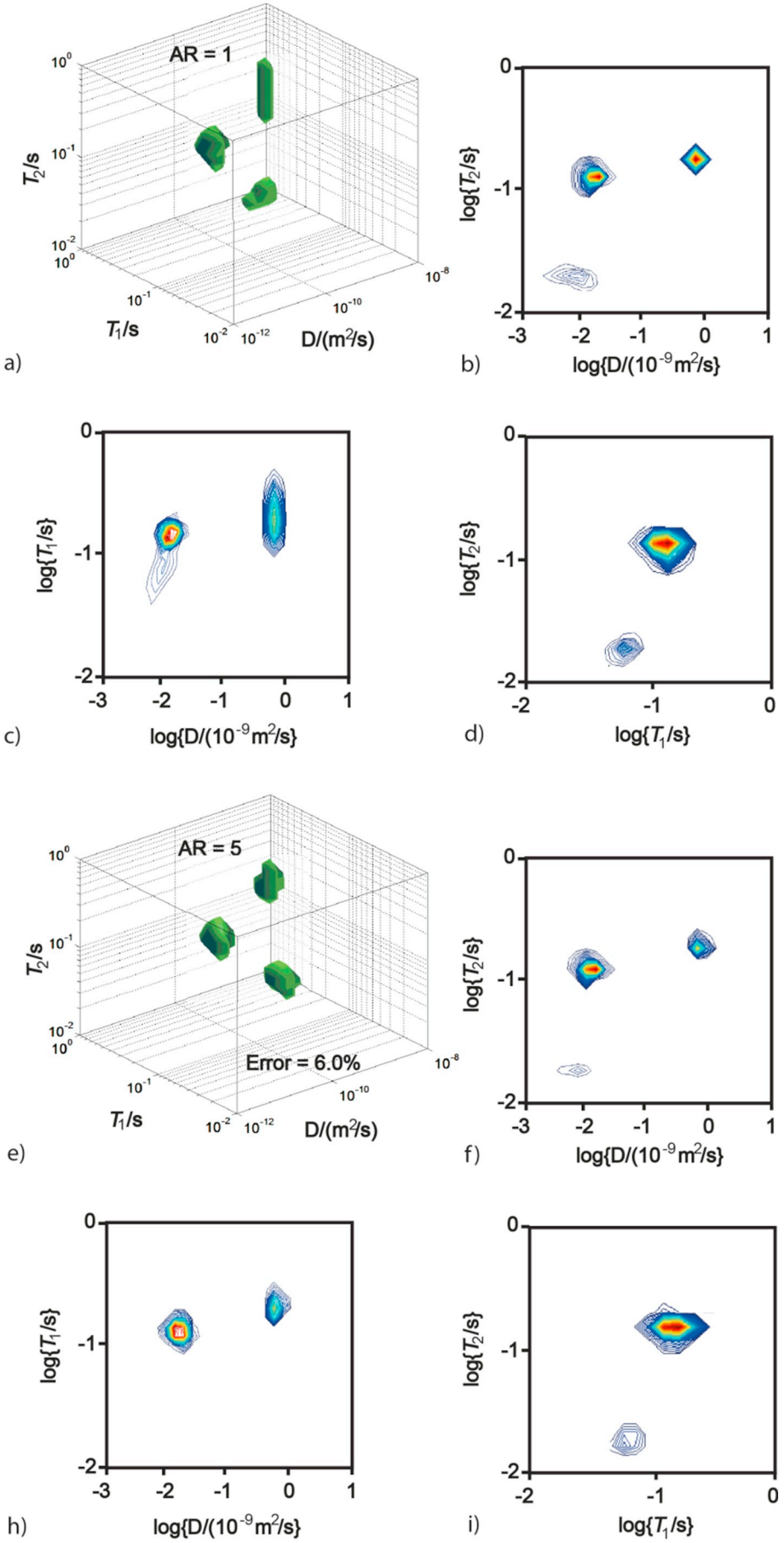

Fig. 6. Experimental results (a)–(d) spectra from fully sampled data. (e)–(h) spectra from subsampled data. The SNR is 23. The oil-water mixture ratio is 1:1 and the glass bead volume fraction is 0.64.

sequence with 100 μs echo time to minimize internal magnetic field effects. The recycle delay, δ and Δ are set to 3 s, 5 ms and 100 ms, respectively. The fully sampled data takes 3 h measurement time and the subsampled data only takes 0.6 h. To further verify the algorithm, simulations were also done. Gaussian noise was used to achieve a signal-to-noise ratio (SNR) of 30. The size of the simulated data is $32 \times 32 \times 64$, which is similar to experimental data. The ratio of amplitude of the two simulated peak is 1:1. The D, T_1 and T_2 for simulation is 2.5×10^{-9} m^2/s, 0.15, 0.1 and 5×10^{-11} m^2/s, 0.6, 0.4, respectively. This is similar to the experimental conditions.

4. Results and discussion

Fig. 3a–d and e–i show the simulation results from fully sampled data and subsampled data, respectively. The T_1–D–T_2 correlation map from fully sampled data (Fig. 3) agrees well with the correlation maps (Fig. 3e) reconstructed from subsampled data with an accelerated ratio (AR) of 5. A relative error of 5.2% is obtained, which means high quality CS reconstruction is achieved. The projected 2D correlation maps from Fig. 3a and e are presented in Fig. 3b–d and f–I respectively to further examine the CS reconstruction. The main pattern of the three projected 2D maps from fully sampled data is also similar to the maps obtained from subsampled data, which confirms the validity of the method.

Subsequently, Figs. 4–6 presents the experimental results. Three peaks are clearly observed in Fig. 4a, one can be attributed to water (with large D) and two others are from oil (with small D). Fig. 4b–d shows the projected D–T_2, D–T_2 and T_1–T_2 correlation maps, respectively. The peak from water indicates restricted diffusion due to a smaller D (around 1×10^{-9} m^2/s). The two oil peaks have similar diffusion coefficient but different relaxation time. This may be due to the different components of two kinds of oil. Diffusion and relaxation are sensitive to different molecule motions: for diffusion translational motion is important and for relaxation rotational motion is important. So the two oil molecules could have similar translational motion ability but different rotational motion ability. The high T_1/T_2 ratio for the peak with smaller T_1, T_2 also suggests that rotational motion of this molecule is slow. Fig. 4e–i presents the results inversed from subsampled data with a relative error of 5.8%. These maps are consistent with the correlation maps from fully sampled data (Fig. 4a–d). In Fig. 4i, the peak with smaller T_1, T_2 shows a positive shift along T_1 direction compared to Fig. 4d, this means that weak peak could be distorted by the CS reconstruction method. The results for oil-water ratio of 1:1 are shown in Fig. 5. The strength of oil peaks in Fig. 5 increases compared to these in Fig. 4, which agrees with the varied oil-water ratio. The glass beads sample with dense packing was also measured (Fig. 6) to examine the sensitivity of this method. Lower SNR is obtained due to lower void volume, which leads to a lower accuracy of CS reconstruction. The correlation map shift to shorter relaxation direction, this may be due to that lower void volume results a higher surface-to-volume ratio.

5. Conclusion

T_1–D–T_2 correlation maps were obtained with the CS reconstruction method to save measurement time. Simulation and experiment were implemented to verify this method. An AR of 5 is achieved with a relative error of around 5% for low SNR NMR data. Three water and oil peaks are clearly distinguished in both fully sampled and subsampled results. This suggests high quality CS reconstruction is obtained. The samples with different oil-water mixture ratio and volume fraction were measured to examine the sensitivity of this method. The potential diffusion and relaxation information are also discussed. It is worth noting that the pseudo 2-D relaxation model can also be used to reduce the measurement time of multidimensional Laplace experiment, which should be compared with CS method in the future to find that which is the proper way in different situations [24,25].

Acknowledgement

Financial Supported by Beijing Natural Science Foundation (8184084), the National Natural Science Foundation of China (Grant No. 21427812), the '111 Program' (B13010), and Science Foundation of China University of Petroleum, Beijing (Grant No. 2462015YJRC003) is gratefully acknowledged.

References

[1] Kleinberg RL, Jackson JA. An introduction to the history of NMR well logging. Concepts Magn Reson Part A 2001;13(6):340–2.
[2] Kleinberg RL. Well logging overview. Concepts Magn Reson Part A 2011;13(6):342–3.
[3] Kleinberg RL. NMR measurement of petrophysical properties. Concepts Magn Reson Part A 2001;13(6):404–6.
[4] Coates GR, Xiao L, Prammer MG. NMR Logging: Principles and Applications. Halliburton Energy Services Publications; 1999.
[5] Dunn KJ, Bergman DJ, Latorraca GA. Nuclear Magnetic Resonance Petrophysical and Logging Applications. Elsevier; 2002.
[6] Cohen MH, Mendelson KS. Nuclear magnetic relaxation and the internal geometry of sedimentary rocks. J Appl Phys 1982;53:1127–35.
[7] Kleinberg RL, Horsfield MA. Transverse relaxation processes in porous sedimentary rock. J Magn Reson 1990;88:9–19.
[8] Allen DF, Flaum C, et al. Trends in NMR logging. Oil Field Rev 2000;12:2–19.
[9] Timur A. Pulsed nuclear magnetic resonance studies of porosity, movable fluids, and permeability of sandstone. J Pet Technol 1969;21:775–86.
[10] Kenyon WE, Day PI, Straley C, Willemsen JE. A three-part study of NMR longitudinal relaxation properties of water-saturated sandstones. SPE Form Eval 1988;3:622–36.
[11] Mitchell J. Rapid measurements of heterogeneity in sandstones using low-field nuclear magnetic resonance. J Magn Reson 2014;240:52–60.
[12] Mitchell J, Gladdena LF, Chandraseker TC, Fordham EJ. Low-field permanent magnets for industrial process and quality control. Prog Nucl Magn Reson Spectrosc 2014;76:1–60.
[13] Mitchell J, Howe AM, Clarke A. Real-time oil-saturation monitoring in rock cores with low-field NMR. J Magn Reson 2015;256:34–42.
[14] Li M, Xiao D, Romero-Zerón L, Marica F, et al. Mapping three-dimensional oil distribution with π-EPI MRI measurements at low magnetic field. J Magn Reson 2016;269:13–23.
[15] Ming L, Vashaee S, Romero-Zerón L, et al. A magnetic resonance study of low salinity waterflooding for enhanced oil recovery. Energy Fuel 2017;31:10802–11.
[16] Venkataramanan L, Song Y, Hurlimann MD. Solving Fredholm integrals of the first kind with tensor product structure in 2 and 2.5 dimensions. IEEE Trans 2002;50:1017–26.
[17] Hürlimann MD, Venkataramanan L. Quantitative measurement of two-dimensional distribution functions of diffusion and relaxation in grossly inhomogeneous fields. J Magn Reson 2002;157:31–42.
[18] Song Y, Venkataramanan L, Hürlimann MD, Flaum M, Frulla P, Straley C. T_1–T_2 correlation spectra obtained using a fast two-dimensional Laplace inversion. J Magn Reson 2002;154:261–8.
[19] Sun BQ, Dunn KJ. A global inversion method for multi-dimensional NMR logging. J Magn Reson 2005;172:152–60.
[20] Arns CH, Washburn KE, Callaghan PT. Multi-dimensional inverse Laplace NMR spectroscopy in petrophysics1. Petrophysics 2007;25(4):548–9.
[21] Mobli M, Hoch JC. Nonuniform sampling and non-Fourier signal processing methods in multidimensional NMR. Prog Nucl Magn Reson Spectrosc 2014;83:21–41.
[22] Lustig M, Donoho D, Santos JM, Pauly J. Compressed sensing MRI. IEEE Signal Process Mag 2008;25(2):72–82.
[23] Zhang Y, Xiao L, Liao G. Accelerated 2D Laplace NMR with compressed sensing at low SNR, Microporous Mesoporous Mater.
[24] Williamson NH, Röding M, Galvosas P, et al. Obtaining T_1-T_2 distribution functions from 1-dimensional T_1 and T_2 measurements: the pseudo 2-D relaxation model. J Magn Reson 2016;269:186–95.
[25] Williamson NH, Röding M, Liu H, Galvosas P, et al. The pseudo 2-D relaxation model for obtaining T_1-T_2 relationships from 1-D T_1 and T_2 measurements of fluid in porous media. Microporous Mesoporous Mater 2018;269:191–4.